Soft Matter

This article can be cited before page numbers have been issued, to do this please use: J. Liu, D. Sychev, N. Davydiuk, M. Al-Hussein, A. Fery and Q. A. Besford, *Soft Matter*, 2025, DOI: 10.1039/D4SM01454E.

View Article Online
DOI: 10.1039/D4SM01454E

ARTICLE

Hybrid Phytoglycogen-Dopamine Nanoparticles as Biodegradable Underwater Adhesives

Jiayi Liu[a], Dmitrii Sychev[a], Nadiia Davydiuk[a], Mahmoud Al Hussein[a,b], Andreas Fery[a] and Quinn A. Besford[a]*

Received 00th January 20xx,
Accepted 00th January 20xx

DOI: 10.1039/x0xx00000x

Developing adhesive materials that can selectively degrade into non-toxic by-products, is a key challenge in the materials sciences, particularly for short-term implantable devices and tissue regeneration treatments. Herein, we leverage biodegradable phytoglycogen (PG) nanoparticles (highly-branched glucose polysaccharide nanoparticles) as scaffolds for coupling adhesive dopamine motifs to be used as biodegradable underwater adhesives. The phytoglycogen-dopamine (PG-dopa) hybrid nanoparticles could be synthesised in aqueous solvent, to which the products retained a similar size and particle morphology to the initial PG nanoparticles. The PG-dopa nanoparticles could readily be assembled into dense monolayers on silica substrates through a simple dip-coating procedure. Colloidal probe atomic force microscopy was used to characterise the adhesiveness underwater, where it was found the films produced strain energy release rates towards 8 mJ/m^2 between hard silica materials. Importantly, the PG-dopa films retained the original biodegradability towards glucosidase enzymes, which can degrade the adhesives in fluids containing these enzymes over time (e.g., 45 U/mL of α-amylase solution degraded the majority of the adhesive films in 30 min). Given the inherent biocompatibility of glycogen materials, we anticipate these adhesives having application in short-term implantable devices.

Introduction

Mussel feet secrete adhesive proteins that help them firmly stick to rocks in marine environments, where the adhesive proteins form plaques on the substrates. A linear protein (mefp-5) with an average molecular weight of about 10 kDa, plays a significant role in forming robust mussel plaques, especially in the strong interface connection[1, 2]. The adhesion ability of mefp-5 is mainly due to L-dopa, which contains a functional catechol group. Hydrogen bond, metal-coordination and hydrophobic interaction can form between these catechol groups and substrates resulting in strong interface adhesions[3, 4].

These unique underwater adhesive properties of L-dopa have inspired the development of synthetic underwater or wet adhesives, which might find application in the biomedical field. For example, synthetic polymers that mimic mussel adhesive proteins have shown high underwater adhesion strengths[5-7]. Cui et al. developed a starch-based tissue adhesive by using dopamine-conjugated starch. This dopamine modified starch can form a hydrogel when hydrogen peroxide with horseradish peroxidase is used as a cross-linker. Catechol groups served as interfacial adhesion and crosslinking segments[8]. Du et al. reported a mechanical and chemical robust coating using catechol-modified polyallylamine. The catechol group and amine group contribute to the strong interface adhesion on several substrates and cohesive interaction by forming covalent bonds. The abundant amine groups on the coating provide grafting sites for secondary modification[9]. Whilst these materials have demonstrated unique adhesive properties, there is interest to move towards minimally synthetic, bio-sourced materials as adhesives. Furthermore, for applications involving bio-contact (e.g., implants, tissue adhesives), biocompatibility is necessary. Glycogen is an interesting material in this regard, which has been gaining momentum in various applications[10], particularly as it has been shown to induce minimal inflammation, coagulation, and interactions with the immune system in human blood[11].

Glycogen is a randomly hyperbranched polysaccharide nanoparticle that can be obtained from various sources (animals, tissues, plants). Its structure consists of repeating D-glucose units connected by linear α-(1,4) glycosidic linkages, with branching via α-(1,6) glycosidic linkages. The nanoparticle size, molecular weight, degree of branching and content of protein are different depending on the source. For instance, phytoglycogen (PG) derived from sweet corn has a diameter of ~80 nm in water and high molecular weight of 20 MDa[12](Figure 1a). The hydroxyl groups on glycogen can be modified to produce other functional groups, such as carboxylic acid group[13], quaternary ammonium group[14], and allyl groups[15], as examples. The glucose residues can be oxidized to produce an aldehyde group, which can be further reacted with primary amines to conjugate functional groups[16]. Previous works have investigated thiolated glycogens as mucosal adhesives, and as gold-adhering

a. Leibniz-Insitut für Polymerforschung Dresden e.V., Hohe Str. 6, 01069 Dresden, Germany
b. Physics Department, The University of Jordan, Amman 19942, Jordan.
*E-mail: besford@ipfdd.de

nanoparticles[17], which have demonstrated robust properties of adhesive glycogen. Coupling the unique properties of glycogen, with underwater adhesive catechol motifs, has not been pursued, to our best knowledge.

Herein, we report a rapid and easy method to form underwater PG adhesive coatings using PG-dopamine (PG-dopa) hybrids, inspired by the mussel foot protein (Figure 1a). PG nanoparticles, which are sourced from plants (sweet corn kernels), are hydrophilic and have no ability to adhere to substrates underwater[17]. However, we found that PG-dopa nanoparticles show remarkable affinity to silicon dioxide surfaces. A homogenous coating consisting of a single layer PG-dopa nanoparticles can be formed by a simply dip coating into PG-dopa dispersions. The PG-dopa coating showed great adhesiveness to silicon dioxide materials underwater. The maximum average adhesion energy reached 7.20 mJ/m^2. Previously, the values as high as 2.64 mJ/m^2 were reported for dopa-containing mussel-inspired proteins[18]. The modification of dopamine did not affect the biodegradability of PG-dopa nanoparticles or coatings. We anticipate these adhesives to have use in short-term implantable devices.

Methods

Materials. Phytoglycogen (PG) sourced from the kernels of sweet corn was purchased from Mirexus (Guelph, Canada). Sodium periodate (≥99.8%), dopamine hydrochloride (≥98%), sodium cyanoborohydride (≥95%), 4-methycatechol (≥95%), α-amylase (powder, ~30 U/mg), phenol (≥99%) and deuterium oxide (≥99.9%) were purchased from Sigma-Aldrich. Sulfuric acid (≥95%) was purchased from Fisher Chemical. Ethanol absolute was purchased from VWR chemicals. Methyl sulfoxide (99.7+%) was purchased from Thermo Scientific. Dialysis tube (14000 Daltons cut-off) was purchased from BioDesign Inc. of New York. High-purity (Milli-Q) water with resistivity of 18.2 MΩ cm was obtained from a Direct-Q® 3UV water purification system (Merck Chemicals GmbH, German).

Synthesis of PG-dopa. PG-dopa was synthesized by the Schiff base reaction between dopamine and oxidized PG and then reduced by sodium cyanoborohydride. We synthesized some different conjugates (percentage modifications of PG). Here we describe the 10% modification (10% of glucose units of PG modified). PG (0.2433 g, 1.50 mmol) was dispersed in 10 mL of Milli-Q water by ultrasonication. Then sodium periodate (0.0321 g, 0.15 mmol) was added and the dispersion was stirred for 2 h at room temperature in the dark. The dispersion was dialyzed (14 kDa cutoff) against Milli-Q water one night to remove the oxidizing agent. The dispersion was transferred to a round bottom flask. The flask was sealed by rubber septum and degassed with argon 20 minutes. Dopamine hydrochloride (0.0569 g, 0.30 mmol) was dissolved in 5 mL phosphate buffer (0.1 M, pH 5) and was added to the oxidized PG dispersion. After 4 h, sodium cyanoborohydride (0.0471 g, 0.75 mmol) was dissolved in 5 mL phosphate buffer (0.1 M, pH 5) and was added to the reaction dispersion for one night. Subsequently, the dispersion was precipitated in 40 mL ethanol twice. The precipitate dispersed in 20 mL Milli-Q water again and dialyzed (14 kDa cut-off) against Milli-Q water for 3 days. Finally, the dispersion was freeze-dried to obtain the PG-dopa10%. The degree of conjugation was determined by ^1H NMR spectrum and catechol group assay.

View Article Online
DOI: 10.1039/D4SM01461F

Nuclear Magnetic Resonance Spectroscopy (NMR). ^1H spectra were collected on a Avance III HD 500 MHz spectrometer (Bruker, Germany). Deuterium oxide (D_2O) was used as solvent.

Catechol group assay. The UV-vis absorbance spectra were recorded on a SPECORD 40 spectrophotometer (Analytik Jena, Germany) and analyzed using the software WinASPECT. Spectra were acquired with a scan speed of 20 nm/s. A constant 0.005 mg/mL Iron (III) chloride solution, 4-methylcatechol solution concentration range from 0.01 mg/mL to 0.08 mg/mL and total volume 2 mL carbonate buffer solution (0.1 M, pH 8.3) samples are prepared for the standard absorbance curve. In detail, a fresh 0.05 mg/mL Iron (III) chloride and 1 mg/mL 4-methylcatechol water solution were prepared as stock solutions. To prepare the sample with 4-methylcatechol concentration 0.01 mg/mL, 0.2 mL 0.05 mg/mL Iron (III) chloride solution, 0.02 mL 1 mg/mL 4-methylcatechol solution and 1.78 mL Milli-Q water was add to the PMMA cuvette. The sample with higher 4-methylcatechol concentration was prepared by increasing the volume of 1 mg/mL 4-methylcatechol solution and decreasing the volume of Milli-Q water. The volume of 0.05 mg/mL Iron (III) chloride solution and total volume are always 0.2 mL and 2 mL. The cuvettes were put in the chamber for the measurement after the solution became homogeneous. A wavelength range from 300 to 800 nm was used.

The PG-dopa5%, PG-dopa10% and PG-dopa15% nanoparticles were dispersed in carbonate buffer solution (0.1 M, pH 8.3) with the help of ultrasonication 30 minutes. All the concentration are 0.8 mg/mL. To prepare the PG-dopa samples for UV-vis spectrometer, 0.2 mL 0.05 mg/mL Iron (III) chloride solution and 1.8 mL 0.8 mg/mL PG-dopa5% or PG-dopa10% or PG-dopa15% solution was added to the cuvette. The cuvettes were put in the chamber for the measurement after the solution became homogeneous. A wavelength range from 300 to 800 nm was used.

To compare the absorbance intensity of PG-dopa samples with 4-methylcatechol standard absorbance curve, the absorbance intensity at wavelength 525 nm was used.

Preparation of PG-dopa10% coating on silicon wafer. The PG-dopa10% coating on silicon wafer was obtained by dip coating in a 1 mg/mL PG-dopa10% Milli-Q water dispersion without waiting time. The lift speed is 0.048 mm/s. The coated wafer was rinsed by Milli-Q water to remove the unbounded PG-dopa10% nanoparticles.

Atomic force microscopy (AFM). AFM topography measurement on nanoparticles and coatings were performed in peak-force mode on a Dimension Fastscan AFM (Bruker, Billerica, MA, USA) with a peak-force set point of 30 mV. Tap300 Al-G cantilever (40 N/m, 300 kHz, coated by 30 nm Aluminium, BudgetSensors) were employed. All measurements were performed consecutively with the same type of cantilever. The obtained data were processed by Gwyddion software. To obtain the PG and PG-dopa10% nanoparticle AFM topography images, 0.005 mg/mL nanoparticle water dispersion was prepared. 0.1 mL water dispersion was applied to the silicon wafer and dried by slow nitrogen flow. For the thickness of PG-dopa coating on silicon wafer, several scratches were prepared by using a small syringe needle.

Dynamic light scattering (DLS). Hydrodynamic diameter and zeta potential were measured using a Zetasizer Nano-ZS instrument (Malvern Instrument. Malvern, UK). The concentration of both PG and PG-dopa water dispersion are 1 mg/mL.

Scanning electron microscopy (SEM). SEM images were recorded using NEON40 SEM (Carl Zeiss Microscopy Deutschland GmbH, Oberkochen, Germany) operated at acceleration voltage of 1 kV. No additional conductive coating was necessary to prevent charging of the specimen in the electron beam.

Cryo-transmission electron microscopy (cryo-TEM). Cryo-TEM images were recorded in Libra 120 microscope (Carl Zeiss Microscopy Deutschland GmbH, Oberkochen, Germany). 4 µL of the specimen was placed onto a holey carbon TEM grid (Quantifoil R3.5/1, 300 mesh), blotted with filter paper and vitrified in liquid ethane at -178 °C using a Grid Plunger (Leica Microsystems GmbH, Wetzlar, Germany). Frozen grids were transferred into Gatan 626 (Gatan GmbH, München, Germany) cryo-TEM holder. Images were recorded at an accelerating voltage of 120 kV while keeping the specimen at -170 °C.

X-ray reflectivity. X-ray reflectivity measurements were performed using XRD 3300 T-T (Seifert) diffractometer with a copper target (λ = 0.154 nm). The samples were mounted horizontally at the center of a two-circle goniometer and investigated under specular reflection conditions from 0 to 6°. At specular reflectivity the scattering vector, $q = (4\pi/\lambda)\sin\theta$, is perpendicular to the film (*z*-direction), where 2θ is the scattering angle. Hence, the reflected intensity is sensitive to the electron density profile averaged over the footprint of the incident X-ray beam.

PG-dopa coating underwater adhesion measurements by colloidal probe AFM. Adhesion measurements were carried out using an atomic force microscope (MFP-3D, Asylum Research, Oxford Instruments, California, USA). The colloidal probe atomic force microscopy (AFM) technique was utilized to measure the adhesion force and quantify adhesion interactions[19, 20]. This technique allows quantitative measurements of the adhesion interaction between adhesive PG-dopa coating and a 20 µm diameter silica spherical particle, the colloidal probe. The advantage of using the micrometer size sphere as an indenter is the defined geometry of the contact, unattainable in the case of the hard tip[21]. The borosilicate glass slides with No.1 thickness (VWR, Radnor, USA) were coated with adhesive PG-dopa film and used as a sample for the AFM measurements. To fabricate the colloidal probe equipped cantilever, the tipless cantilever (CSC 36, Mikromasch Europe, Wetzlar, Germany) was calibrated using the thermal noise technique[22] prior to the attachment of the colloidal probe by micromanipulator, resulting in a spring constant of 2.51 N/m. Adhesion characterization was carried out by recording the force-distance curves with different maximal loads on the cantilever (50 nN, 100 nN, 215 nN), contact times (0.5-50 s), and the retraction rates (100 nm/s - 5000 nm/s). It is worth noting that the retraction rate was 2000 nm/s unless stated otherwise. The measurement was carried out by recording a 4 x 4 point force map on an arbitrarily chosen position on the sample. For every parameter set, two such force maps were recorded (one for the PG-dopa15% coating). Due to the comparable adhesion of the PG-dopa film between the borosilicate glass substrate and the silica colloidal probe, as the functional groups are the same, the material transfer interfered with the measurements, resulting in the measurement of cohesion and adhesion interactions mixture. To overcome this issue, the parameters of the measurement were varied in different directions for each of the force maps (i.e. for the first set of force maps the load was consecutively increased and for the second set it was consecutively decreased). Within this set, the measured adhesion force (the minimum on the retraction part of the force curve) decreased after several force curves had been recorded. To measure only the adhesive interactions, the values after such drop were omitted, and the cantilever was treated with O_2 plasma to achieve a greater contribution of the adhesion interactions to the measured force.

Adhesion was quantified by integrating the part of the force curve below zero on the retraction part of the force curve and normalising it to the calculated area of contact from maximal deformation within the framework of Johnson-Kendall-Roberts theory[23]. The measurements were conducted at room temperature in Milli-Q water.

Degradation of PG and PG-dopa nanoparticles by α-amylase solution. The enzymatic degradation of PG and PG-dopa10% was assessed using a phenol-sulfuric acid assay[11, 24]. Dispersions of both nanoparticles in Milli-Q water with a concentration of 1 mg/mL were prepared. α-amylase was dissolved in PBS buffer (0.01 M, pH 7.4) and the concentration is 1 U/mL. To begin the assay, 70 µL PG or PG-dopa dispersion was added to 200 µL enzyme solution. The resulting solution was incubated at 23 °C with gentle agitation for 3 h. Then, the undigested PG and enzyme were separated from the free glucose using spin columns with a pore size of 10 kDa. The filtrate was collected and divided into sample aliquots of 50 µL, to which concentrated sulfuric acid (150 µL) was added, followed by addition of 5wt% phenol water solution. The samples were subsequently incubated at 90 °C with agitation for 20 minutes. The UV-vis absorbance of the digested solution was then measured at 490 nm with an infinite M200 microplate reader (Tecan, Switzerland) using a 96-well plate (Greiner CELLSTAR, sigma-Aldrich).

To determine the amount of glucose on each particle type, the original PG on each particle type, the original PG solutions (70 µL) were each treated with 0.2 M TFA (200 µL) for 3 h at 80 °C with agitation. The mixtures were then treated and analyzed as described above for the enzymatic experiments. The extent of degradability was determined as the ratio of UV-vis absorbance reading intensity at 490 nm for the enzymatically degraded particles to the trifluoroacetic acid degraded particles.

Fluorescence. Fluorescence of the PG-dopa coatings was analysed with a JASCO FP-8500 spectrofluorometer instrument. A quartz surface was cut into a 10 mm strip, and coated with PG-dopa10% nanoparticles. This was then placed inside a quartz cuvette with 4 mL solution, on a 45 ° angle to the excitation source, and the detection channel (situated perpendicular to each other). The emission wavelength of excitation spectrum was 340 nm. The excitation wavelength of emission spectrum was 280 nm. The excitation wavelength and emission wavelength for the fluorescence intensity of PG-dopa10% coated quartz over time in the solution of α-amylase are 280 nm and 310 nm.

View Article Online
DOI: 10.1039/D4SM01454E

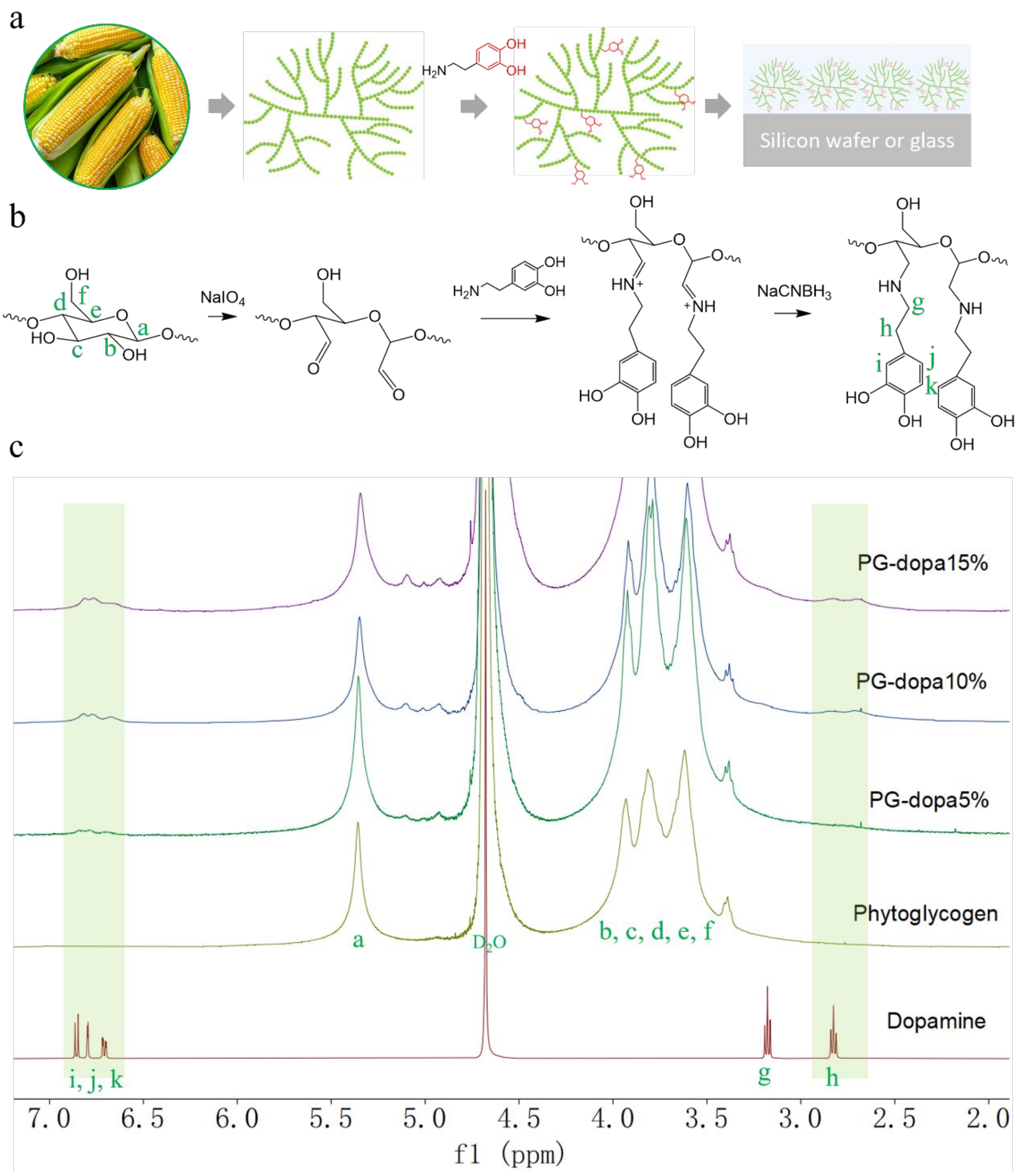

Figure 1. a) Phytoglycogen (PG) extracted from sweet corn and monolayer dopamine-conjugated phytoglycogen (PG-dopa) on substrates. b) the synthesis scheme of PG-dopa. c) ^1H NMR (600 MHz, D_2O) spectra of dopamine, PG, PG-dopa5%, PG-dopa10% and PG-dopa15%.

Result and discussion

Synthesis of PG-dopa. The PG was first oxidized by sodium periodate to produce aldehyde group[25]. Then the dispersion was purified by dialysis to remove the oxidizing agent. The aldehyde group in oxidized PG was reacted with the amine of dopamine hydrochloride in phosphate buffer (pH 5.0). Finally, the imine was reduced to a stable secondary amine by reductive amination (Figure 1b).

The successful synthesis and degree of conjugation was confirmed by ^1H NMR spectroscopy. The i, j and k peaks at δ ~ 6.8 ppm were assigned to the protons from the aromatic ring of dopamine, which indicated the presence of the catechol group on the modified nanoparticles (Figure 1c). The methylene protons (g and h) from dopamine hydrochloride can also be found at δ 3.1 and 2.8 ppm after modification. The degree of conjugation (DC) of dopamine of the PG-dopa was calculated by the equation $DC{=}A_{6.8}/(3{\times}A_{5.3})$, - where $A_{6.8}$ and $A_{5.3}$ are the integrations of the peak area at δ = 6.8 (aromatic protons) and δ = 5.3 (the proton at the C1 of glucose repeat unit, a peak), respectively. The DC of different PG-dopa is summarized in Table 1. The number in the term PG-dopa10% is the ratio (mol:mol) of sodium periodate and glucose repeat unit. The degree of conjugation of PG-dopa10% was found to be 4.67%. However, the broadness of the NMR peaks makes absolute quantification difficult for such low conjugation degrees.

Table 1. Conjugation degrees of PG-dopa determined by ^{1}H NMR and catechol assay.

Samples	Degree of conjugation (%)	
	^{1}H NMR	Catechol assay
PG-dopa5%	2.67	3.35
PG-dopa10%	4.67	5.22
PG-dopa15%	6.00	7.31

Given the broadness of the peaks, the degree of conjugation was additionally confirmed by a catechol assay. The 4-methylcatechol was used to obtain the standard curve over the concentration range of 0.01 - 0.08 mg/mL (Figure S1b). The UV-vis absorbance intensity at wavelength 525 nm was used to plot the fitting curve (Figure S1d). For purpose of the assay, we assume the molecular weight of glucose repeat unit does not change after the conjugation of dopamine. Then the DC can be calculated by the following equation.

$$DC = \frac{C_{cat} \times M_{gru}}{C_{dcg} \times M_{4mc}} = 1.6327 \times C_{cat}$$

C_{cat} is the concentration of the catechol group in the PG-dopa dispersion. Taking the PG-dopa10% for instance, C_{cat} is 0.0320 mg/mL from the fitting curve (Figure S1d). M_{gru} is the molecular weight of glucose repeat unit in PG, which is 162.1407 g/mol. C_{dcg} is the concentration of dopamine in the conjugate PG, found to be 0.8 mg/mL in this experiment. M_{4mc} is the molecular weight of 4-methylcatechol and is 124.1372 g/mol. The DC of PG-dopa5%, PG-dopa10% and PG-dopa10% were 3.35%, 5.22% and 7.31% (Table 1).

Characterization of PG and PG-dopa nanoparticles. Atomic force microscopy (AFM) was used to measure the dry state morphology and height of PG and PG-dopa10% nanoparticles (Figure 2a and 2b, respectively). The height of both PG and PG-dopa10% nanoparticles was ~12 nm from AFM topography images (Figure S2). It should be noted that the AFM measurements were done in a dry state, which were then compared to cryo-transmission electron microscopy (TEM) and dynamic light scattering (DLS) which were in frozen and liquid water, respectively. Cryo-TEM images of PG and PG-dopa10% nanoparticles (Figure 2c and d, respectively) revealed the shape of the nanoparticles at high resolution, which are consistent with an irregular sphere. The DLS revealed a shift in the intensity peak towards larger hydrodynamic diameters, where the Z-average diameter increased from ~72 nm to ~110 nm, and the dispersity (PDI) also increased from 0.084 to 0.239 (Table S1). Given the bias of DLS towards larger particles, we computed the average diameters of both particle types from the cryo-TEM images (Figure 2f). We found that the PG nanoparticles had diameters in the range of 40 nm to 45 nm, whereas for PG-dopa10% this increased slightly towards 50 nm to 55 nm. This indicated the average size increased after modification. Furthermore, the column graph shape of PG nanoparticles was sharper than that of PG-dopa10% nanoparticles, indicating that the size distribution also increased after modification. This trend was consistent with the diameter population distribution curve from DLS measurements (Figure 3e). The graph shows the relative intensity of scattering light of the nanoparticles with different sizes. We note that the diameters between cryo-TEM and DLS are different in definition (observable size vs. hydrodynamic size). The PG-dopa10% nanoparticles were found to be negatively charged with a zeta potential of -15.0 mV, possibly due to the deprotonation of the catechol groups. The negatively charged can aid the nanoparticle stability in water.

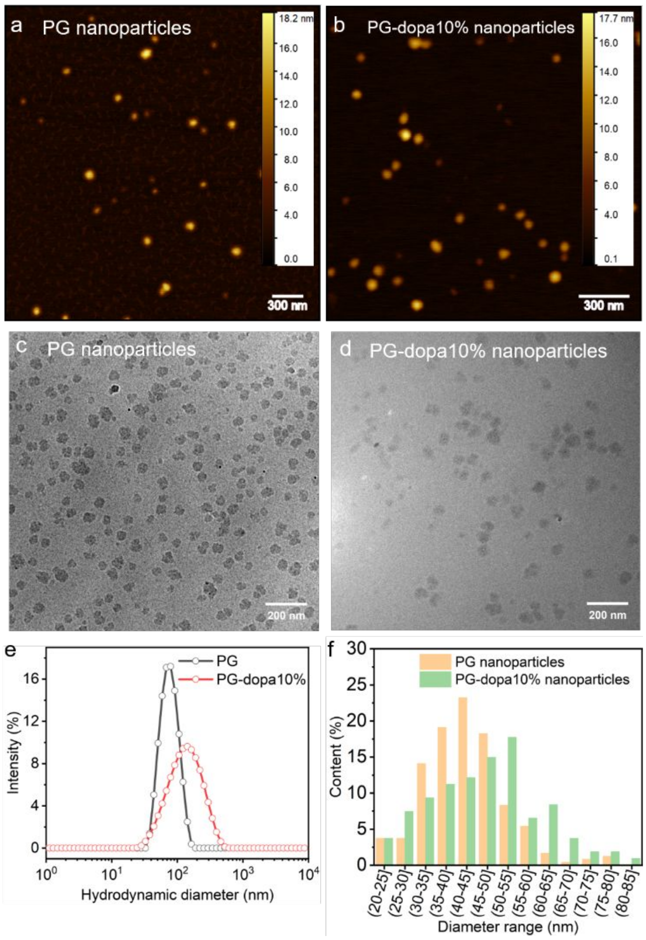

Figure 2. a) Dry state AFM topography image of PG nanoparticles. b) Dry state AFM topography image of PG-dopa nanoparticles. c) TEM image of PG nanoparticles. d) TEM image of PG-dopa10% nanoparticles. e) DLS hydrodynamic diameter populations of PG and PG-dopa nanoparticles. f) Calculated diameter range populations of PG and PG-dopa10% nanoparticles from figure 3c and 3d.

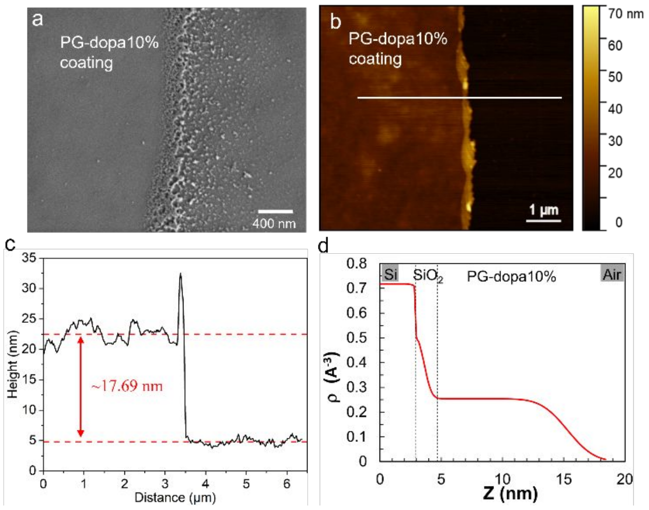

Figure 3. a) The SEM image of PG-dopa10% coating on silicon wafer prepared by dip coating (the left part is the coating and the edge of the coating is in the middle). b) AFM topography image of a scratch of PG-dopa10% coating on silicon wafer. c) The height of white line in AFM topography image. d) XRR curve of PG-dopa coating on silicon wafer. The inset shows the electron density profile extracted from the best fit of the XRR curve.

Morphology and thickness of PG-dopa10% coating. Scanning electron microscopy (SEM) was used to observe the PG-dopa10% coating on silicon wafers. The coating was continuous and smooth (the left area of Figure 3a), whereas the edge of the film (limit of the dip-coating) was porous, with some aggregate nanoparticles. This indicated that the PG-dopa10% nanoparticles showed affinity to the silica material and the interaction between nanoparticles are negligible. AFM topography image revealed that a continuous, dense PG-dopa10% coating of ~18 nm in thickness formed on the silicon wafer by dip coating into the PG-dopa10% water dispersion (Figure 3b and 3C). The thickness of the PG-dopa10% coating was slightly larger than the height of individual PG-dopa10% nanoparticles (~12 nm) (Figure S2), from AFM topography images but less than the double height of the nanoparticles. To obtain further insight into the structure of PG-dopa and PG-dopa coating, Wide-angle X-ray scattering and X-ray reflectivity measurements were performed using established methods[26].Figure S3a,b shows the amorphous nature of the PG-dopa10% which is significantly different from crystalline cellulose fibres. Shown in Figure S4 are the obtained X-ray reflectivity curve together with its corresponding fit data. The weakly damped Kiessig fringes observed throughout the curve indicated a relatively smooth surface with a uniform coating thickness. A good fit of the experimental curve was obtained using a single-layer model onto a thin native silicon oxide layer with a thickness of 0.74 nm. The electron density profile used to obtain the best fit (Figure 3d) corroborates the uniformity of the coating with thickness and rms roughness of 11.7 nm and 1.7 nm, respectively.

DOI: 10.1039/D4SM01491E

The underwater adhesion performance of PG-dopa coatings. The colloidal probe AFM technique was used to characterize the adhesion properties of the PG-dopa10% coating underwater (Figure 4a). A colloidal probe (spherical silica particle with a 20 µm diameter) was brought into contact with PG-dopa coatings on glass substrates, and the force-distance curves were recorded, in water solution. Figure 4b shows a schematic representation of the force distance curve from our experiments. The contact time as well as the maximal load on the cantilever and the retraction rate were varied. As shown previously, the thermodynamic work of adhesion in the case of the interactions of soft polymeric bodies is often very challenging to measure due to the very rapid pull-off event and requires specific experimental setups that are not suitable for every experimental system[27]. In order to avoid misunderstanding, we use here the strain energy release rate G instead of the work of adhesion, as we use a pull-off experiment to determine the adhesion properties of the PG-dopa coatings. The strain energy release rate G, the area on the retraction part of the force-distance curve (Figure S6) below zero normalized on the calculated area of contact, was used to characterize the adhesion performance of the PG-dopa coatings (Figure 4c, d).

View Article Online
DOI: 10.1039/D4SM01454E

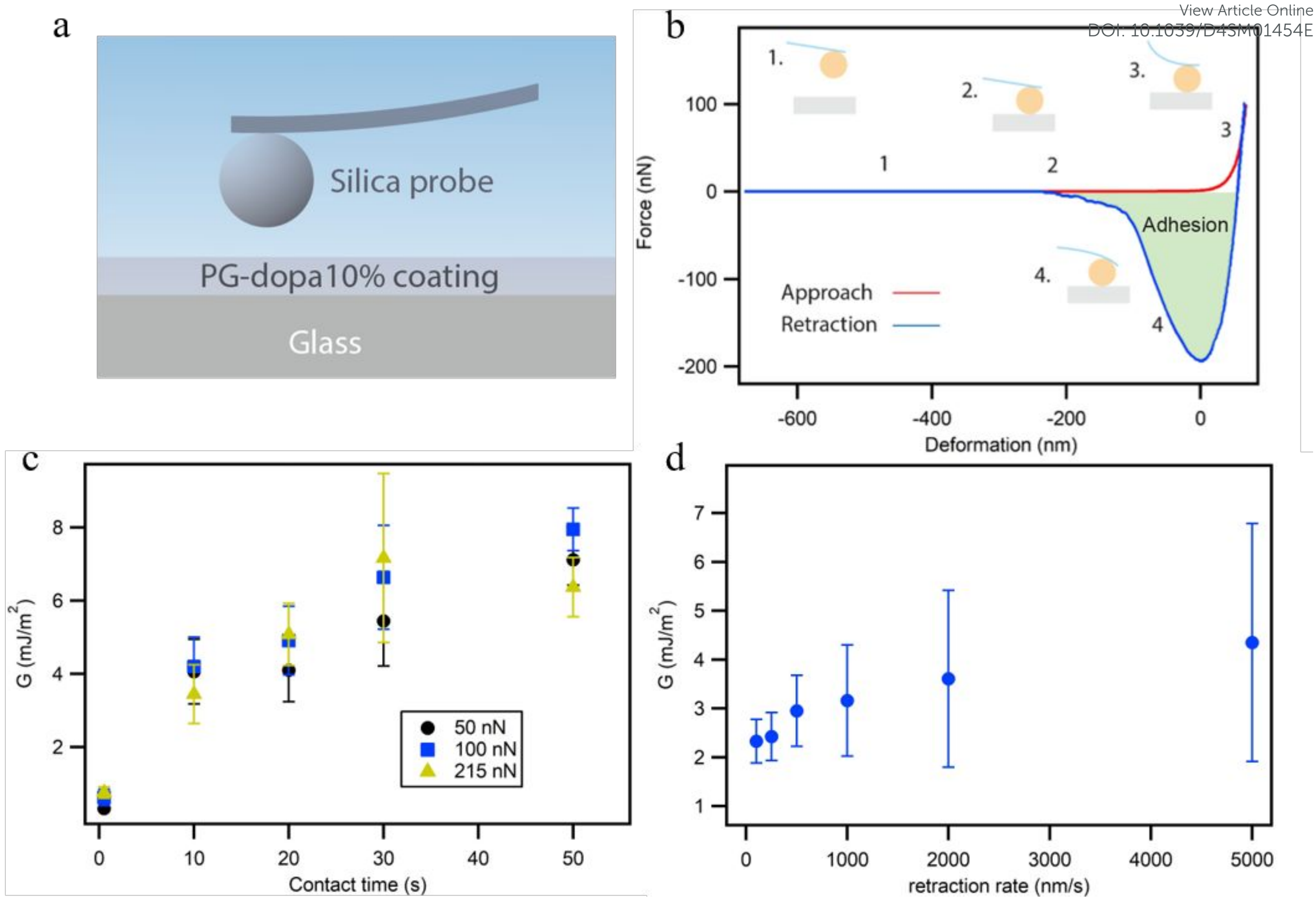

Figure 4. a) Schematic of colloidal probe AFM measurement setup. b) A typical force-deformation approaching and retraction curve from our colloidal probe AFM experiment of PG-dopa10% films. c) The strain energy release rate *G* of PG-dopa10% coating dependence on contact time for maximal load force. d) strain energy release rate of the PG-dopa10% coating as a function of retraction rate.

In the case of the interaction of the soft bodies, the increase of adhesion on contact time, retraction rate, and maximal load is very common[27-30]. Longer contact time allows additional bonds and interactions between the two surfaces to develop. Larger maximal loads increase the deformation of the soft bodies, thereby increasing the contact area and the total number of bonds between the two surfaces. Higher retraction rates is connected with the higher rates for the separation of two surfaces influencing the pull-off force drastically[31, 32]. In our case, the increase of the contact time results in a drastic increase of *G* from below 1 mJ/m² to around 7 mJ/m² on average for each maximal load used (Figure 5c).

While the data for the influence of the retraction rate on *G* have a large standard deviation due to the deposition of the matter on the colloidal probe, which is inevitable in the case of the single particle experiment, the trends can still be seen. The average values of *G* more than doubled from 100 nm/s to 5000 nm/s.

The influence of the maximal load, however, was insignificant in our case. The reason for this behavior can be understood by comparing the maximum deformation of the PG-dopa10% coating generated at each maximal load (Figure S5). The increase of the maximal load did not result in substantial increase in the deformation. The load applied to a soft deformable surface causes a certain amount of deformation. The simplest theory describing the relationship between the applied load F and the resulting deformation δ is the Hertz model. According to this model, $F \sim \delta^{3/2}$. Thus, an increase in load should cause additional deformation. The fact that the deformation remains the same and is not zero suggests that a very hard substrate (glass) is covered by a relatively soft layer. This layer is deformed until the colloidal probe reaches the glass substrate. After that, the cantilever is too soft to indent and measure the deformation of the glass and the silica colloidal probe. Therefore, the maximal load of 50 nN was sufficient to reach the glass substrate under the PG-dopa10% coating. The resulting values of the maximum deformation in this case can be used as an indication of the thickness of the PG-dopa10% coating under water. The maximum deformation of the coating was around 75 nm (Figure S5), which is consistent with the nanoparticle size from the DLS measurements.

The adhesion performance of different PG-dopa coatings was also characterized, namely PG-dopa5% and PG-dopa15% (Figure S7). PG-dopa5% showed very low adhesion and made the interactions of the colloidal probe with the substrate weaker than in the case of

View Article Online
DOI: 10.1039/D4SM01454E

the borosilicate glass (data not shown). PG-dopa15% showed comparable performance to PG-dopa10% at all contact times except 50s, where the adhesion of PG-dopa15% was about 50% greater than that of PG-dopa10%. However, comprehensive investigation of the adhesion performance of PG-dopa15% was limited by the very high colloidal probe contamination, which was significantly greater than that of PG-dopa10%. The thickness of PG-dopa15% was close to that of PG-dopa5% and less than that of PG-dopa10% (Figure S8 and S9). An increased tendency for colloidal probe contamination in the case of PG-dopa15% and lower thickness compared to PG-dopa10% may indicate the lower layer uniformity and stability of PG-dopa15%.

Degradation of PG-dopa10% nanoparticle and PG-dopa10% coatings. The degradation of PG and PG-dopa10% nanoparticles in a 1 U/mL α-amylase PBS solution (pH 7.4, 0.01 M) over 3 h were assessed using a phenol-sulfuric acid assay (Figure 5a). It was found that the functionalized PG-dopa nanoparticles retained a good biodegradability towards α-amylase as the starting material PG nanoparticles. The PG-5% and PG-10% nanoparticle even showed a higher degradation degree than PG nanoparticles. To glean insight into the degradability of the PG-dopa films, a different assay was needed, due to an inability to ascertain the exact amount of PG-dopa10% in the films. We found that the PG-dopa10% has fluorescent properties, whereby under 280 nm excitation, significant fluorescence was observed, peaking at 310 nm (Figure 5b). This emission maximum at 310 nm was used to assess the degradability of the films in real-time, after soaking in α-amylase (45 U/mL) solution (Figure 5c). It was found that there was a kinetic decrease in the fluorescence of the film, decreasing from ~1800 counts and saturating at abut ~500 counts in 30 minutes. This highlights that the adhesive PG-dopa materials are still biodegradable towards glucosidase enzymes with time.

The lyophilised PG-dopa10% was found to be stable under refridgeration for years. The color of the PG-dopa10% water dispersion changed from slightly white foggy to slightly brown (Figure S10a) because of the gradually oxidization of the catechol group[33]. However, no aggregated particles are observed from DLS hydrodynamic diameter population after stroing in the 4 °C fridge for a week or 9 months (Figure S10b). The reason for decreasing of PG-dopa10% particle size after 9 months might be the degradation of glycogen nanoparticle itself over time.

Together, these underwater adhesive nanoparticles can offer a renewable biomaterial alternative to highly synthetic mussel-foot protein mimics, where the degradability yields glucose and a small amount of dopamine. Our study has focused on contact between ideal surfaces (plane and smooth sphere), how it changes between rough surfaces is not yet known. Furthermore, the adhesiveness towards other materials, such as soft, elastic tissues, is currently the subject of our future investigations.

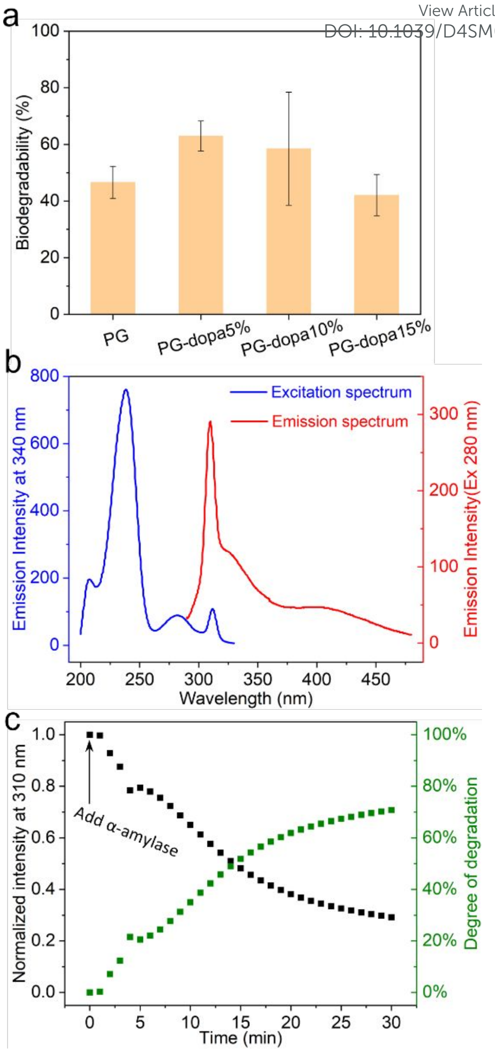

Figure 5. a) The degradation of PG and PG-dopa nanoparticles in 1 U α-amylase PBS solution after 3 h. b) fluorescence excitation and emission spectra of PG-dopa10% films. c) PG-dopa10% coated quartz incubated in α-amylase (45 U/mL) PBS solution, with fluorescence intensity monitored as a function of time. The excitation and emission wavelength are 280 nm and 310 nm.

Conclusions

We have reported on the synthesis of phytoglycogen-dopamine hybrid materials. The catechol group of dopamine endowed the phytoglycogen nanoparticles with an ability to adhere to silicon dioxide materials underwater. It was shown that the phytoglycogen-dopamine nanoparticles adsorbed on silicon dioxide substrates and formed continuous monolayers from a water dispersion. The thickness of the coating was found to be ~18 nm in the dry state, and ~78 nm in water when solvated. The adhesive properties of the coating were striking, with a maximum strain energy release rate of 7.2 mJ/m^2 when contacting surfaces of silicon dioxide underwater. Moreover, the modification did not affect the biodegradability of phytoglycogen. This sticky phytoglycogen coating might find application in short-term implantable devices or as a “micro” adhesives for the assemble of nanoparticles.

Acknowledgments

We sincerely thank Dr. Petr Formanek and Michael Göbel for assistance with TEM and SEM measurements, respectively, and Dr. Hartmut Komber for NMR measurements. The authors additionally would like to thank Dr. Alexander Münch, Qiong Li and Dr. Ilka Hermes for their help with UV-vis spectroscopy and AFM measurements, and Thomas Witzmann and Dr. Günter Auernhammer for discussions. M.A.H. thanks the University of Jordan and Leibniz-Institut for Polymer Research Dresden (IPF Dresden) for financial support. This work received funding from the European Union's Horizon 2020 research and innovation program under the Marie Skłodowska-Curie grant agreement 872233 ("PEPSA-MATE"). J.L. gratefully acknowledges the Chinese Scholarship Council (CSC) for funding.

References

1. E. W. Danner, Y. Kan, M. U. Hammer, J. N. Israelachvili and J. H. Waite, *Biochem.*, 2012, **51**, 6511-6518.
2. J. H. Waite and X. Qin, *Biochem.*, 2001, **40**, 2887-2893.
3. H. Lee, N. F. Scherer and P. B. Messersmith, *PNAS*, 2006, **103**, 12999-13003.
4. H. Lee, S. M. Dellatore, W. M. Miller and P. B. Messersmith, *Science*, 2007, **318**, 426-430.
5. M. A. North, C. A. Del Grosso and J. J. Wilker, *ACS Appl. Mater. Interfaces*, 2017, **9**, 7866-7872.
6. J. Yu, B. Cheng and H. Ejima, *J. Mater. Chem. B*, 2020, **8**, 6798-6801.
7. B. Cheng, J. Yu, T. Arisawa, K. Hayashi, J. J. Richardson, Y. Shibuta and H. Ejima, *Nat. Commun*, 2022, **13**, 1892.
8. R. Cui, F. Chen, Y. Zhao, W. Huang and C. Liu, *J. Mater. Chem. B*, 2020, **8**, 8282-8293.
9. Z. Du, F. Qiao, L. Tong, W. Zhang, X. Mou, X. Zhao, M. F. Maitz, H. Wang, N. Huang and Z. Yang, *Innovation*, 2024, **5**.
10. Q. A. Besford, *Soft Matter*, 2024, **20**, 3577-3584.
11. N. Davydiuk, V. Londhe, M. F. Maitz, C. Werner, A. Fery and Q. A. Besford, *Nanoscale*, 2024, DOI: 10.1039/D4NR03034F.
12. Q. A. Besford, F. Cavalieri and F. Caruso, *Adv. Mater.*, 2020, **32**, 1904625.
13. T. Isogai, T. Saito and A. Isogai, *Biomacromolecules*, 2010, **11**, 1593-1599.
14. S. A. Engelberth, N. Hempel and M. Bergkvist, *Bioconjug. Chem.*, 2015, **26**, 1766-1774.
15. M. Rabyk, M. Hruby, M. Vetrik, J. Kucka, V. Proks, M. Parizek, R. Konefal, P. Krist, D. Chvatil, L. Bacakova, M. Slouf and P. Stepanek, *Carbohydr. Polym.*, 2016, **152**, 271-279.
16. M. Perrone, A. Lopalco, A. Lopedota, A. Cutrignelli, V. Laquintana, J. Douglas, M. Franco, E. Liberati, V. Russo, S. Tongiani, N. Denora and A. Bernkop-Schnürch, *Eur. J. Pharm. Biopharm.*, 2017, **119**, 161-169.
17. P. Pacchin Tomanin, J. Zhou, A. Amodio, R. Cimino, A. Glab, F. Cavalieri and F. Caruso, *J. Mater. Chem. B*, 2020, **8**, 4851-4858.
18. S. Arias, S. Amini, J. Horsch, M. Pretzler, A. Rompel, I. Melnyk, D. Sychev, A. Fery and H. G. Börner, *Angew. Chem. Int. Ed.*, 2020, **59**, 18495-18499.
19. H.-J. Butt, *Biophys. J.*, 1991, **60**, 1438-1444.
20. W. A. Ducker, T. J. Senden and R. M. Pashley, *Nature*, 1991, **353**, 239-241.
21. Y. Jiang and K. T. Turner, *Extreme Mech. Lett.*, 2016, **9**, 119-126.
22. J. L. Hutter and J. Bechhoefer, *Rev. Sci. Instrum.*, 1993, **64**, 1868-1873.
23. K. L. Johnson, K. Kendall, A. D. Roberts and D. Tabor, *Proc. R. Soc. A: Math. Phys. Eng. Sci.*, 1971, **324**, 301-313.
24. Q. A. Besford, A. C. G. Weiss, J. Schubert, T. M. Ryan, M. F. Maitz, P. P. Tomanin, M. Savioli, C. Werner, A. Fery, F. Caruso and F. Cavalieri, *ACS Appl. Mater. Interfaces.*, 2020, **12**, 38976-38988.
25. M. Bertoldo, G. Zampano, L. Suffner, E. Liberati and F. Ciardelli, *Polym. Chem.*, 2013, **4**, 653-661.
26. M. Al-Hussein, Y. Séréro, O. Konovalov, A. Mourran, M. Möller and W. H. de Jeu, *Macromolecules*, 2005, **38**, 9610-9616.
27. D. Sychev, S. Schubotz, Q. A. Besford, A. Fery and G. K. Auernhammer, *J. Colloid. Interface Sci.*, 2023, **642**, 216-226.
28. I. U. Vakarelski, A. Toritani, M. Nakayama and K. Higashitani, *Langmuir*, 2001, **17**, 4739-4745.
29. R. Buzio, A. Bosca, S. Krol, D. Marchetto, S. Valeri and U. Valbusa, *Langmuir*, 2007, **23**, 9293-9302.
30. D. Pussak, D. Ponader, S. Mosca, T. Pompe, L. Hartmann and S. Schmidt, *Langmuir*, 2014, **30**, 6142-6150.
31. D. Maugis and M. Barquins, *J. Phys. D Appl. Phys.*, 1978, **11**, 1989.
32. A. N. Gent and J. Schultz, *J. Adhes.*, 1972, **3**, 281-294.
33. J. Ju, S. Jin, S. Kim, J. H. Choi, H. A. Lee, D. Son, H. Lee and M. Shin, *ACS Appl. Mater. Interfaces*, 2022, **14**, 25115-25125.

View Article Online
DOI: 10.1039/D4SM01454E

Data available within the article. The authors confirm that the data supporting the findings of this study are available within the article.